Comparison between bond crushing energy and fracture energy of rocks in a jaw crusher using numerical simulation

by A. Refahi*, J. Aghazadeh Mohandesi†, and B. Rezai†

Synopsis

For predicting the energy consumption during the size-reduction process, the Bond approach is often used. In this work, the PFC3D discrete element method (DEM) software was employed to model the crushing behaviour of some rocks with different mechanical properties in a laboratory jaw crusher. FLAC3D software was adopted to analyze the stress distribution in the rocks. The rocks studied were modelled as granular assemblies in the shape of a sphere and/or a cube located between two jaws, and the work done by the jaws in the crusher was determined. Nine different types of rocks were studied and the energies consumed by the crusher were compared to those of the Bond comminution energy estimated from the Bond index. There is considerable difference between Bond crushing energy and work done by the jaw crusher for rocks. It appears that the Bond approach is not a suitable method for predicting single particle fracture energy done by the crusher. To verify the results obtained from DEM models, the fracture behaviour of the crushed rocks was examined and was compared to the PFC3D results. The tensile mode of fracturing is favourably modelled by the PFC3D software while the delamination mode cannot be well modelled by PFC3D software.

Keywords: jaw crusher; discrete element method; crushing energy; Bond index

Introduction

The discrete element method (DEM) was first proposed by Cundall and Strack to model the behaviour of soil particles subject to dynamic loading conditions[1]. Mishra and Rajamani pioneered the application of DEM to grinding mills and demonstrated that despite the fact that the DEM simulations are based on two dimensions (2D), the technique is able to predict the power draw of mills with reasonable accuracy over a wide range of mill diameters[2,3]. More than 10 years since then, the DEM technique has been successfully applied to ball mills[4–7], SAG mills[8–10] and centrifugal mills[11,12].

DEM has also been applied to study impact-induced particle breakage. Using DEM simulation of impact breakage of agglomerates[13–15] and aggregates that are hardened by cement[16–18], different parameters that influence the impact fracture have been analysed. In some studies, the finite element method (FEM) is usually adopted to determine stress patterns, and DEM has been used to show crack distributions in rocks under loading[18]. Also, using DEM modeling of the compressive strength and drop weight test, the relationship between strain rate, impact energy and the degree of fragmentation has been determined[19].

Several attempts have been made to model the crushers; Djordjevic *et al.* modelled two types of impact crushers: the vertical- and horizontal-shaft impact crusher. They investigated the effects of the machine design and operational condition on velocity and energy distributions of collision inside the milling chamber, and also on the particle breakage behaviour[20].

In the present study a three-dimensional (3D) particle flow code (PFC3D), based on the DEM technique, has been employed to model the fracture behaviour and crushing energy of different rocks in a laboratory jaw crusher. Also, Fast Lagrangian Analysis of Continua in three dimensions (FLAC3D), based on the finite difference method (FDM), was adopted only to analyse the stress distribution in the rock specimen at the initial contact between the specimen and the jaws.

Nine rocks with different mechanical properties were modelled as granular assemblies in the shape of a sphere and/or a cube. Each rock as a single particle was modelled while it was crushed in a laboratory jaw crusher, and its fracture behaviour in the processing zone was studied using PFC3D software. To verify the estimated results, the fracture mechanisms of the rocks in the jaw

* *Department of Engineering, Zanjan University, Zanjan, Iran.*

† *Mining and Metallurgical Engineering Department, Amirkabir University of Technology, Tehran, Iran.*

 SA ISSN 0038–223X/3.00 + 0.00. Paper received Mar. 2009; revised paper received Sep. 2009.

crusher were studied, and the results were discussed with respect to the fracture behaviour modelled by PFC3D software. Then, the determined work done by the jaws of the crusher were compared with those of the Bond crushing energies (estimated from the Bond crushability index) of the rocks. Also, the effect of the Bond crushability index on the estimated crushing energy of the rocks was studied.

Materials and methods

In this work, nine different rock specimens were obtained from some mines in Iran. The mechanical properties (elasticity modulus and uniaxial compressive strength) and the Bond crushability index of these rocks were experimentally evaluated. For this purpose a standard compaction test was carried out on five cylindrical specimens of 54 mm diameter and 135 mm height using an Instron servo hydraulic machine. To measure the modulus of elasticity, five strain gauges were used. The Bond index was estimated using a standard impact crushability test that was applied to 15 cubic specimens of height 50 mm. The dry density of the rocks studied was estimated by the saturation and caliper technique, which was defined by the International Society for Rock Mechanics (ISRM). The Bond crushability index, uniaxial compressive strength, elasticity modulus and dry density of the rocks studied are shown in Table I.

Generally, there are three Bond indices: ball, rod and crushability. The Bond ball and rod indices are determined using standard ball and rod mill, respectively, and are suitable for grinding. The Bond crushability index, which is estimated using a standard impact crushability test, is suitable for crushing[21]. Because the jaw crusher was modelled in this study, the Bond crushability index of the rocks studied was determined.

To study fracture mechanisms of the rocks in the processing zone of a crusher, a cubic and a spherical specimen of limestone were prepared, and their fracture process in a laboratory jaw crusher were studied using a high-speed camera.

Table I

Mechanical properties of the rocks studied

Rocks	Bond index $\frac{kWh}{tonne}$	Uniaxial compressive strength MPa	Elasticity modulus GPa	Density $\frac{tonne}{m^3}$
Amphibole	21.9	130	58.4	2.17
Biotite	22.4	150	63.6	2.6
Black-shale	14.4	60	11.3	2.21
Diorite	20.4	117	46.9	2.31
Granite	18.9	100	45.2	2.16
Grano diorite	19.3	120	53.1	2.34
Porphyry grano diorite	16.3	93	40	2.31
Rhyolite	15.7	86	28.5	2.42
Limestone	12.8	52	26	2.09

PFC3D model of rock and jaw crusher

In order to examine the fracture behaviour of the rocks and to determine the applied energy in a jaw crusher, a PFC3D model of a jaw crusher was developed. This model is a single macro-particle simulation in a crusher, and multi-body interactions are ignored. The crushing process for a single cubic and/or a single spherical rock in the jaw crusher is simulated using the PFC3D model.

It is possible to model the behaviour of particles that may be enclosed within a finite volume by non-deformable walls. The code keeps a record of individual particles and updates any contact with other particles or walls. Each calculation step includes the solution of equations of motion to a particle, using a force-displacement law for each contact[1]. The rock is modelled as an assembly of stiff particles (balls) that are bonded together. The properties of the bonds between balls can be defined in the PFC3D software[22]. For the purpose of modelling, a cubic specimen 5 cm high and a spherical specimen 6 cm in diameter were prepared from nine various rocks that were studied. The rocks were modelled using 3 000–4 000 randomly arranged balls with various diameters of 1.5 to 3 mm (Figure 1).

PFC3D software simulates macro-scale material behaviour from the interactions of micro-scale components, the input parameters are micromechanical properties of constituents, which are listed in Table II[23]. These micromechanical properties cannot be derived directly from measurements of

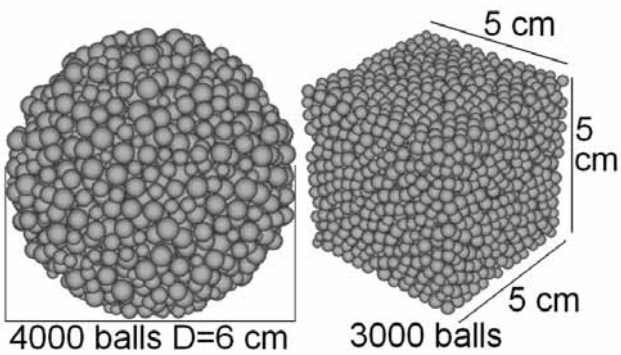

Figure 1—Models of spherical and cubic rocks studied displayed by PFC3D software

Table II

Micromechanical properties of particles and bond strengths used for modelling limestone (determined from simulated uniaxial compaction test by PFC3D)

Ball density ($\tilde{n}_b$)	2090 kg/m^3
Ball-ball contact modulus (E_b)	35 GPa
Ball stiffness ratio (K_n/K_s)	2.5
Parallel-bond modulus ($\bar{E}_c$)	35 GPa
Parallel-bond stiffness ratio ($\bar{K}_n/\bar{K}_s$)	2.5
Ball friction coefficient (Í)	0.70
Parallel-bond normal strength ($\bar{\sigma}_c$)	71 MPa
Parallel-bond shear strength ($\bar{\tau}_c$)	71 MPa

laboratory specimens. To estimate properties of constituent balls and their bonding strength for the purpose of simulating the rocks studied, the corresponding uniaxial compaction test on studied rocks was simulated using PFC3D software; the inputted micro-parameters were changed until the calculated data—elasticity modulus and uniaxial compressive strength from the PFC3D model—matched the estimated data from the experimental uniaxial compaction test. The strength and the elasticity modulus of limestone, which were determined from the simulated uniaxial compaction test, are 52.4 MPa and 25.3 GPa, respectively, matching the experimental values of limestone in Table I. Table II gives the micromechanical properties and bond strengths of Limestone, which are determined by simulating the uniaxial compaction test.

A laboratory jaw crusher was then modelled using the PFC3D code. A jaw crusher has two plates (jaws), one of which is fixed and the other, swinging open and closed, trapping and crushing material between the two surfaces. The feeding entrance is 10 cm wide, and its maximum discharge aperture is 2.5 cm (open status). The minimum open space between the jaws during the crushing cycle is 17 mm (closed status). The rotational speed of the moving jaw is almost 300 rpm. The jaw surface is corrugated; the height and width of a corrugation is 0.5 cm (Figure 2).

Various positions in which a cubic and a spherical specimen may be located in the jaw crusher are shown in Figure 3. For the cubic specimen, two types of contact between a rock and the vertical jaw are possible. These are described as planar and linear.

In order to computing the breakage energy in the DEM model, the concept of wall energy has been utilized. The wall energy is equal to the total accumulated work done by all walls (here the jaws of the crusher) on the granular model of rock specimens that is calculated by the PFC3D software[23]. It is assumed the fracture energy of rocks is equal to the wall energy per mass of rocks. In this case dynamic and multiple impacts behaviour of the crusher has been neglected.

FLAC3D model of jaw crusher

In order to determine the stress distribution in the rocks during crushing, a FLAC3D model similar to a laboratory jaw crusher was developed; spherical and cubic rocks were placed between a vertical and an inclined jaw. In FLAC3D, the continuous medium is replaced by a discrete, equivalent one in which all forces involved are concentrated at the nodes of a 3D mesh used in the medium representation. Then, equations of motion for the continuum are transformed into discrete forms of Newton's equations at the nodes. The resulting system of ordinary differential equations is then solved numerically using an explicit finite-difference approach in time[24]. The FLAC3D models of a cubic and spherical specimen between two rigid jaws are shown in Figure 4.

The jaws are modelled as a rigid medium, and the rocks are modelled as an elastic medium. It is assumed that at the contact surface between specimens and the jaws, no slipping and penetration occurs. The vertical jaw is fixed, and the inclined jaw moves towards the fixed jaw until the distance between these is the limiting value of 17 mm at the bottom (Figure 4). The stress distribution has been estimated for the first stage of the contact.

Modeling fracture behaviour of spherical rocks

When a spherical rock is located between the two jaws, the surface contacts between the rock and the jaws are reduced to small areas that can reasonably well be approximated as points. A severe stress concentration is built up near the contact areas. Figure 5 shows the distribution of major principal stress, estimated from finite-difference analysis, in the limestone specimen at the first contacts; high compact stresses are developed near the contact areas, and tensile stresses are formed in the other parts of the rock.

The fracture progress of a single spherical specimen with 6 cm diameter was photographed by a high-speed camera during the crushing process. Figure 6 gives the fracture mechanism of the spherical limestone in the processing zone of the laboratory jaw crusher. Because the specimens were dropped into the crusher manually, and the crushing process occurs very rapidly, the conductor's fingers are also seen in the pictures.

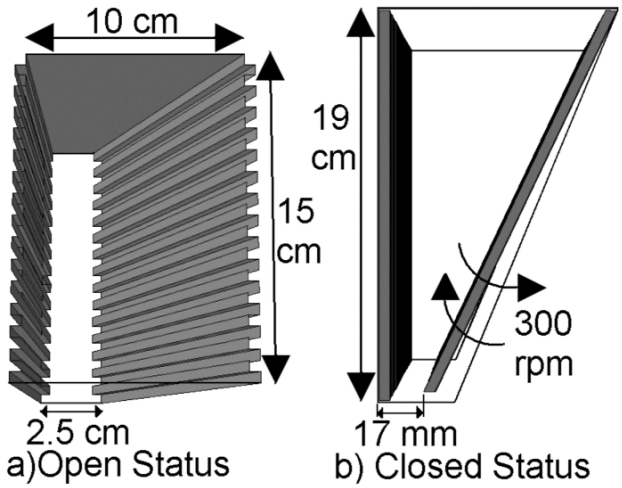

Figure 2—PFC3D model of a laboratory jaw crusher in (a) open and (b) closed status

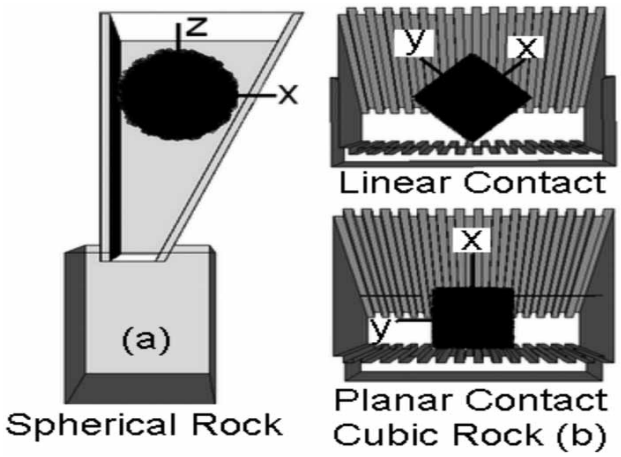

Figure 3—PFC3D model, giving positions of (a) a spherical specimen viewed from the side and (b) a cubic specimen viewed from above in a jaw crusher

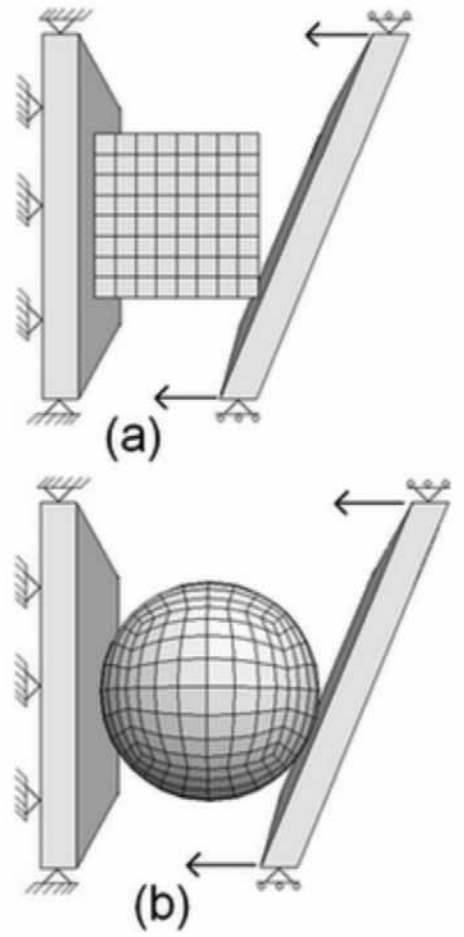

Figure 4—FLAC3D model of (a) a cubic and (b) a spherical specimen between two rigid jaws

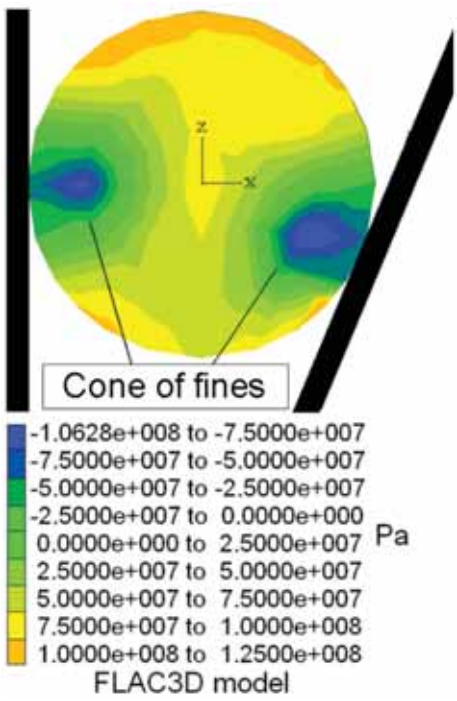

Figure 5—Major principal stress (σ_{max}), determined from finite-difference analysis, acting on a spherical limestone in the plane across the vertical diameter of the sphere

Fine products are often produced in the experiment, as the areas directly below the loading contacts are intensely crushed. Since there is an excess of input energy near the contact areas, finer sized progeny, shown in Figure 6, are produced[25]. High crushing occurs in the areas in which compact stresses are developed (Figure 5). In Figure 5 the transition from compact to tensile stress takes place in the boundary of the semi-elliptical region in which intense crushing with fine products occurs. This region was defined as the cone of fines in which the primary disturbance and crack initiation occur under loading, as is shown in Figure 5. The estimated results are consistent with those of Tomas *et al.*[17]. The cone of fines is usually produced when the surface contact between the loading plate and the rock is close to being a point.

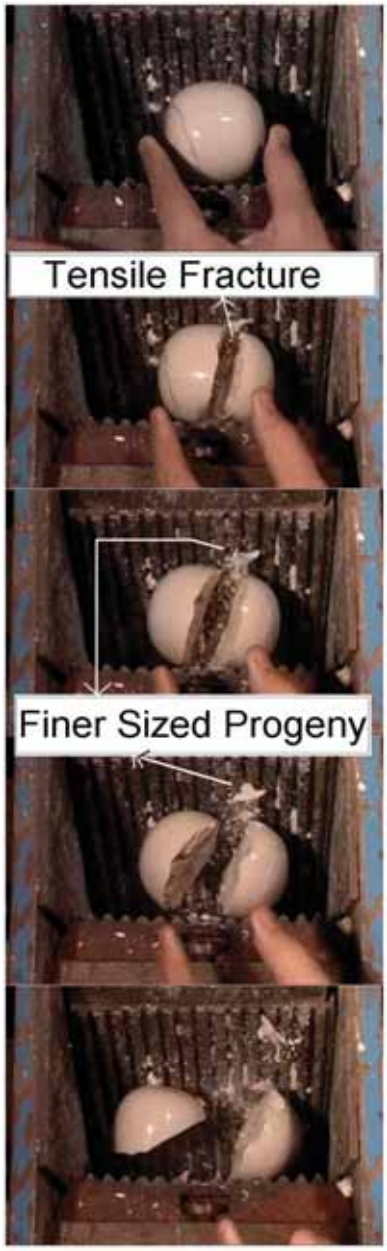

Figure 6—Initial fracture process of a spherical limestone in a laboratory jaw crusher, viewed from above

Figure 7 shows the results of the corresponding DEM simulation of the fracture progress estimated by PFC3D software.

Figures 6 and 7 show that after formation of the cone of fines, the spherical limestone breaks under tensile fracture mode in the near vertical plane in which the dominant major principal stresses are of tensile type (Figure 5). Also, it seems that the tensile mode of fracture is well presented by the DEM in the spherical specimen.

From Figure 6, it is clear that two hemisphere-shaped pieces are produced at the first stage of the crushing process.

Figure 8 represents the following stages of the crushing processes; the hemispherical pieces of limestone tend to be in a stable position in which the contact between the rock and the jaws is confined to a point on one side, and planar contact on the other side. The pattern of stress distribution in the rock in the vicinity of the point of contact is similar to that shown in Figure 5. Accordingly, the fracture mechanism in the hemispherical limestone is again of the tensile mode. Similarly, the fracture mechanism of the rock pieces in the following stages of crushing is tensile, as shown by the PFC3D model (Figure 8). Consequently, DEM is the suitable technique to model fracture of a single spherical rock in the jaw crusher.

If the contacts between the rock pieces and the crushing plates tend to be linear or pointed, the tensile fracture mechanism will become more dominant than the shear-fracture mechanism. On the other hand, where the contact surfaces become planar, the dominant fracture mode may be either shear or a mixed mode of shear and tensile fracture[26]. Also, the corrugated surfaces of the jaws cause higher stress concentration near the contact areas in the rock. The dominant fracture mode under these circumstances is usually tensile. Since the tensile strength of a brittle rock is much less than its shear strength[26], the consumed energy in a jaw crusher containing corrugated jaws decreases. In other words, the higher the brittleness of a rock, the higher is the effect of the stress concentration, reducing the fracture strain energy.

With PFC3D software it is possible to calculate the wall energy applied to a rock by the jaws. Figure 9 shows the wall energy applied to the spherical limestone versus the number of time steps; the maximum wall energy is equal to 237 (joules). Considering the mass of spherical limestone, the consumed energy that is equal to the maximum wall energy per the mass of rock for the size reduction of limestone from 6 to 2.5 cm is almost 1002 (kJ/tonne).

Also, for predicting the energy consumption during the size-reduction process, the Bond relationship, expressed as the following, is often used[27]:

$$W = 10W_i\left(\frac{1}{\sqrt{P_{80}}} - \frac{1}{\sqrt{F_{80}}}\right) \qquad [1]$$

where W_i is the Bond index (kWh/tonne), P_{80} is the size at which 80% of the product passes (in microns), F_{80} is the size at which 80% of the feed passes (in microns) and W is the energy consumption (kWh/tonne). Considering the Bond crushability index of limestone, 12.8 kWh/tonne, the Bond crushing energy of limestone in terms of kJ/tonne is expected to be 1030 (P_{80} = 2.5 × 10⁴ and F_{80} = 6 × 10⁴ microns), which is more than the energy consumption estimated from the PFC3D model.

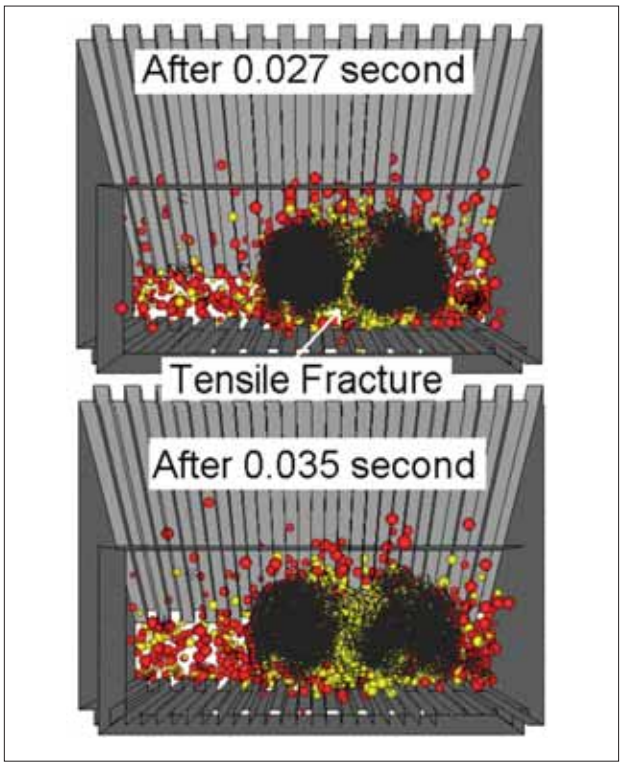

Figure 7—DEM modelling of fracture progress of a spherical limestone in a jaw crusher, viewed from above

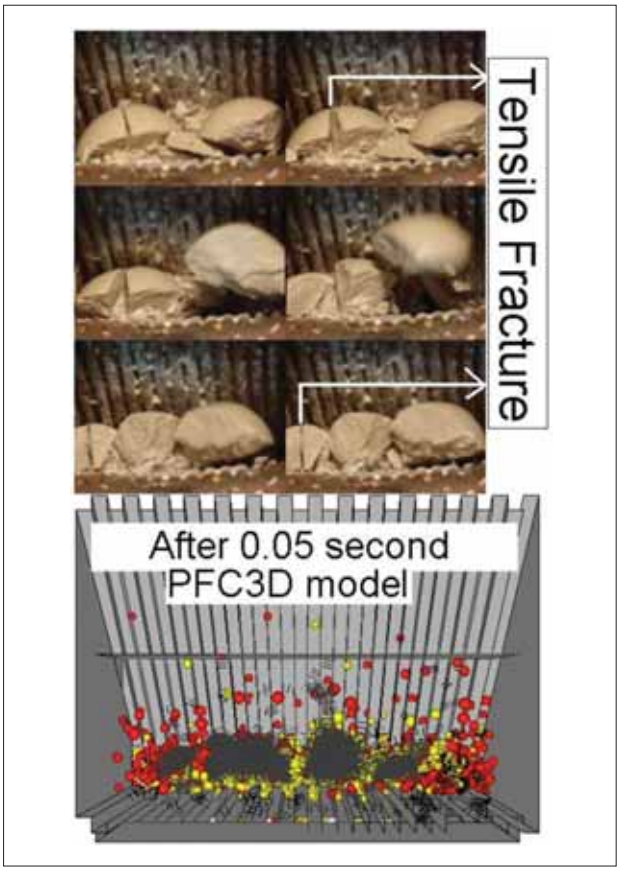

Figure 8—Sequential crushing progress of a spherical limestone in a jaw crusher and DEM model for an intermediate stage of crushing, viewed from above

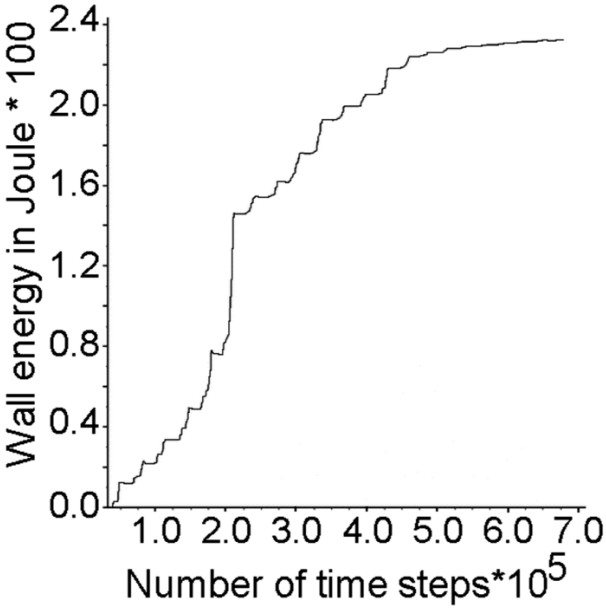

Figure 9—Wall energy applied to a spherical limestone by jaws

Similarly, wall energies that are applied to spherical specimens of each of the rocks studied that were crushed by the jaws have been simulated by PFC3D software. The results, together with the corresponding Bond crushing energies, are shown in Table III. The calculated energy consumed by PFC3D, that are equal to the wall energy per the mass of rocks, is considerably less than the Bond crushing energies for spherical specimens (Table III). Because the model is developed as a single pseudo-static wall deformation episode, it does not accurately correspond to the dynamic and multiple impact behaviour of the experimental crusher. Moreover the kinetic energy of the particle fragments has been neglected. This seems to justify the higher Bond energy rather than the wall energy.

As it is seen from Table III, the harder the rock the higher is the percentage of difference between wall energy per mass of rocks and Bond energy. Because the strain rate in Bond impact crushability test is much higher than the jaw crusher while by increasing the strain rate, in comparison to low-strength rocks, the fracture energy of harder rocks increases considerably[28]. In addition the effect of stress concentration imposed to a harder rock in the corrugated jaw crusher is much more significant. Consequently the change in difference between Bond crushing energy and wall energy are observed.

The remarkable differences between wall energies obtained from PFC3D model and Bond crushing energies show that the Bond equation is not suited to single particle breakage. Consequently, the Bond crushability test cannot successfully predict the power draw of the laboratory jaw crusher for crushing a single spherical rock.

Modelling fracture behaviour of cubic rocks

As shown in Figure 3, a cubic rock may be in several positions in a jaw crusher. Results show that when the contact area between the cubic specimen and the vertical jaw is reduced to a line, the specimen rotates until it is in a stable position before the commencement of the fracturing process (Figure 10).

After the rotation of the cubic specimen, the results from DEM modeling for the cases of linear contacts between a crushed rock and the vertical jaw are similar to those of planar contacts. When the contact area between a cubic rock and the vertical jaw is planar, a delamination mechanism usually occurs. Also, similar to the spherical specimen, an intensely crushed region is formed at the initial point of the contact during the crushing process. Figure 11 shows the major principal stress distribution in the cubic limestone determined by the FLAC3D model. The intensely crushed region where high compact stress is developed is a prism. The prism of fines forms near the linear contact area between a cubic rock and the loading platens (Figure 11).

Table III

Bond crushing energies (calculated from Equation [1]) and wall energy per mass of rock (estimated from PFC3D software) for spherical specimens

Rocks	Bond crushing energy kJ/tonne	Wall energy per mass of rocks kJ/tonne	Percent of difference between wall and bond crushing energy%
Limestone	1030	1002	2.7
Black-shale	1165	1159	0.4
Rhyolite	1263	1152	8.7
Porphyry grano-diorite	1316	1237	5.9
Granite	1520	1407	7.4
Grano-diorite	1556	1309	15.8
Diorite	1645	1432	12.9
Amphibole	1769	1568	11.3
Biotite	1805	1326	26.5

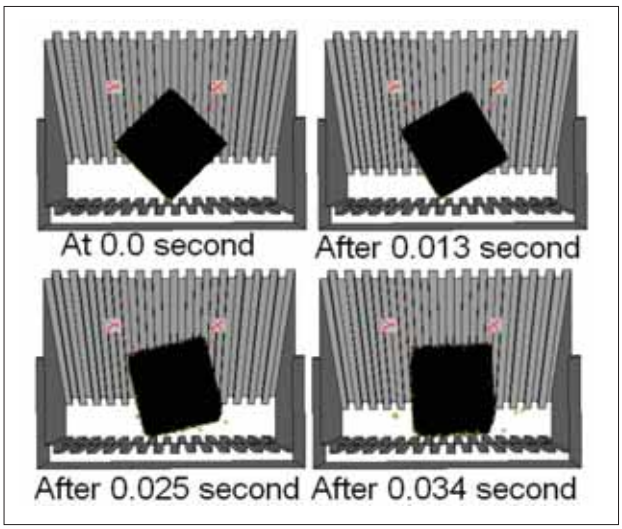

Figure 10—Rotation of a cubic specimen having linear contact with the vertical jaw, viewed from above

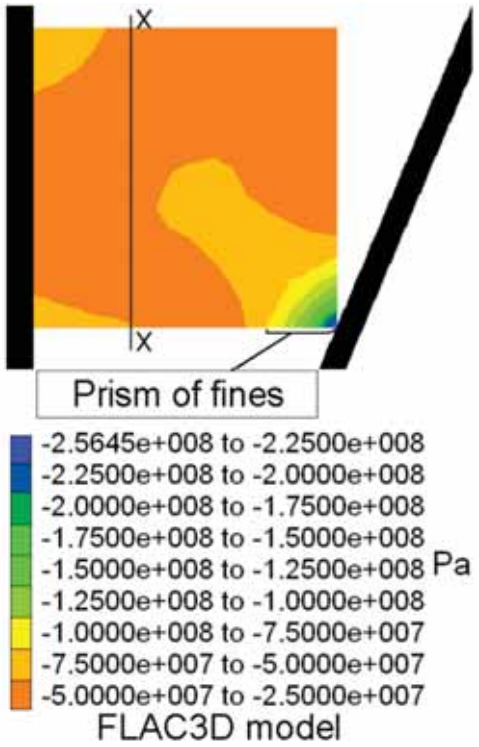

Figure 11—Major principal stress (σ_{max}) in a cubic limestone

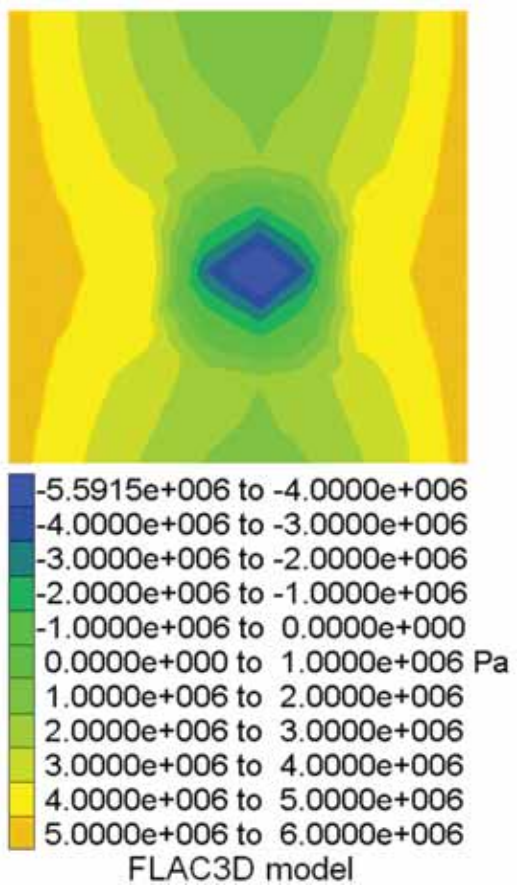

Figure 12—Distribution of lateral principal stress in section x-x of a limestone specimen (σ_{min})

The distribution of the principal lateral stress in the surface of section x-x, which is shown in Figure 11 for limestone, is given in Figure 12 (estimated from FLAC3D model).

Referring to Figure 12, the stress distribution in section x-x of the cubic limestone is such that the lateral tensile-stress component is developed in the specimen. Because the jaw face is corrugated, remarkably high stress concentrations may be developed at the contact surfaces and owing to the combined effect of lateral stress and stress concentration near the circumferences of the specimen, the stress may reach the fracture strength of limestone, thereby making it a favourable site for crack initiation. Growth of the initial crack occurs in the vertical planes, causing delamination. Thin sheets are separated from the circumferences of the limestone, as shown in Figure 13. Figure 14 shows the DEM modelling of the fracture mechanism of the cubic limestone specimen in the jaw crusher.

Referring to Figure 14, it seems that the process of delamination is not convincingly modelled by DEM. It seems that the limitation of DEM model for simulating the delamination process may be inherently due to its disability for stress analysis where the stress is continuum quantity and therefore does not exist at each point in a particle assembly, because the medium is discrete. In the discrete PFC3D model, contact forces and particle displacements are computed. These quantities are useful when studying the material behaviour on a micro-scale, but they cannot be transferred directly to a continuum model[23].

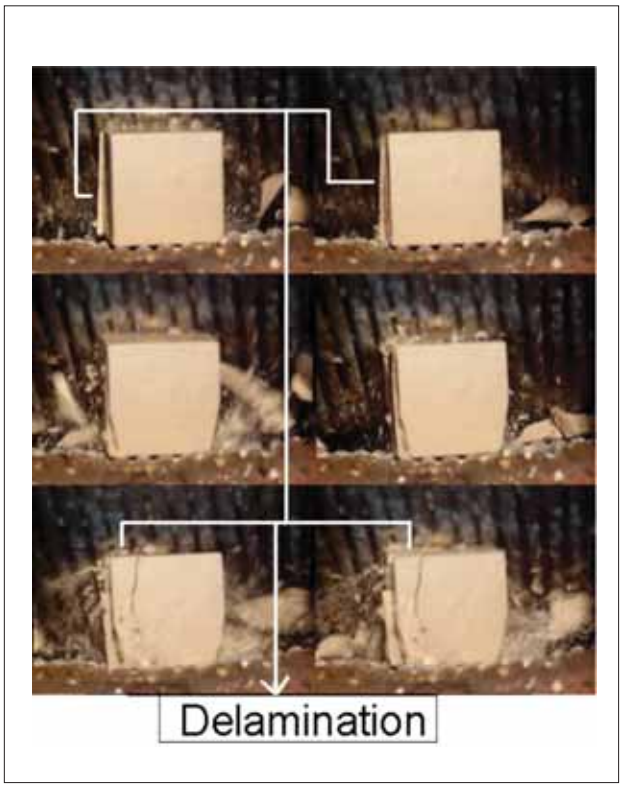

Figure 13—Fracture process for cubic limestone in a laboratory jaw crusher, viewed from above

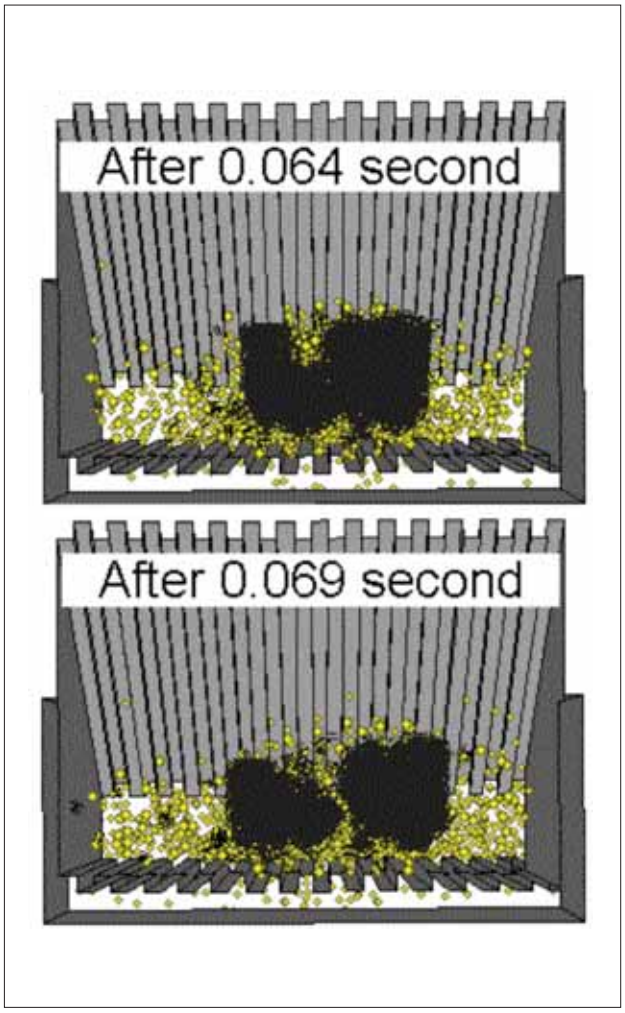

Figure 14—DEM modeling of fracture progress of a cubic limestone in a jaw crusher, viewed from above

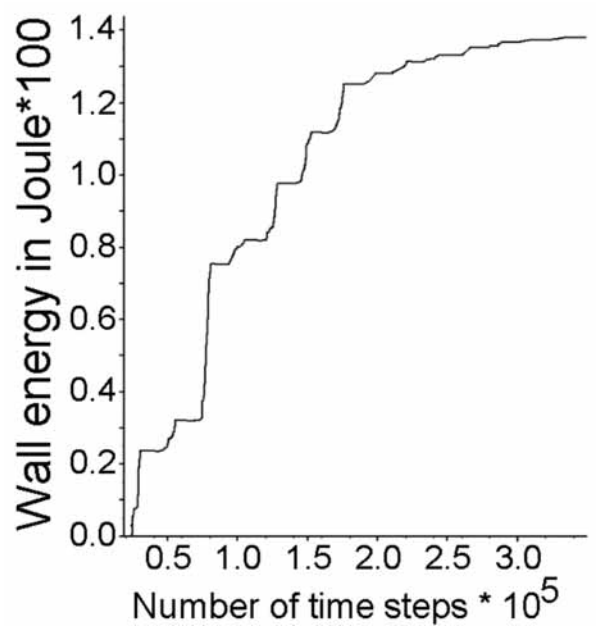

Figure 15—Wall energy applied to a cubic limestone specimen by jaws

Table IV

Bond crushing energies (calculated from Equation [1]0 and wall energy per mass of rock (estimated from PFC3D code) for cubic specimens

Rocks	Bond crushing energy $\frac{kJ}{tonne}$	Wall energy per mass of rocks $\frac{kJ}{tonne}$	Percent of difference between wall and bond crushing energy%
Limestone	852	530	37.8
Black-shale	962	523	45.6
Rhyolite	1043	497	52.3
Porphyry-grano-diorite	1087	532	51.1
Granite	1256	657	47.7
Grano-diorite	1285	620	51.7
Diorite	1358	634	53.3
Amphibole	1461	755	48.3
Biotite	1491	646	56.7

The maximum wall energy applied to the cubic limestone was determined from the PFC3D model and is equal to 138.4 J, as shown in Figure 15. Consequently, the required energy for reducing the size of a cubic limestone from 5 to 2.5 cm is 530 kJ/tonne, which is equal to the maximum wall energy per the mass of limestone, whereas the Bond crushing energy for limestone at P_{80} and F_{80} of 25 000 and 50 000 microns, respectively, is equal to 852 kJ/tonne (calculated from Equation [1]). There is a considerable difference between the crushing energy determined using PFC3D (530 kJ/tonne), and the crushing energy estimated using the Bond index—Equation [1] (852 kJ/tonne)—for limestone.

Similarly, the crushing behaviour of eight other rocks (given in Table I) was studied in the form of cubic specimens and also simulated using PFC3D software. Table IV gives the Bond crushing energy of the rocks and the wall energy per the mass of the rocks. There is remarkable difference between the Bond crushing energy and the wall energy of the cubic rocks. Consequently, like the spherical specimens, the Bond approach is not suitable method for predicting the fracture energy of a single cubic rock.

Conclusion

The results of simulating a jaw crusher using PFC3D for nine different rock types in the sphere and cube shapes confirm that there is remarkable diversity between the wall energies per mass of rocks and the Bond energies of rocks. There is a difference between the Bond and wall energy varying from 2.7% for the lowest-strength rock (spherical limestone rock) to 26.5% for the hardest rock (spherical biotite rock) and from 37.8% for the lowest-strength cubic rock to 56.7% for the hardest cubic rock. Consequently, it seems the Bond equation is not suitable method for estimating fracture energy of a single cubic and/or a single spherical rock. Therefore, the Bond crushability test cannot successfully predict the power draw of the laboratory jaw crusher.

Because the model is developed as a single pseudo-static wall deformation episode, it does not accurately correspond to the dynamic and multiple impact behaviour of the experimental crusher. Moreover the kinetic energy of the particle fragments has been neglected.

The difference between wall and Bond energies for harder rocks are more than those of lower-strength rocks which was due to more sensitivity of hard rocks to stress concentration and strain rate.

The fracture mechanism of the spherical rock is tensile mode and is well predicted by DEM model, unlike the cubic rock where the agreement with the experimental results is not good. The fracture mode of the cubic specimen is delamination in the jaw crusher. Since PFC3D software cannot analyse lateral tensile-stress component in the rock, the process of delamination is not modelled by DEM.

Acknowledgments

The authors would like to acknowledge The Zanjan University for financial support and Mehras Company. Also, the authors wish to acknowledge the assistance of Farzad Refahi for high-speed photography.

References

1. Cundall, P.A. and Strack, O.D.L. A discrete model for granular materials. *Geotechnique*, vol. 1, 1979. pp. 47–56.
2. Mishra, B.K. and Rajamani, R.K. The discrete element method for simulation of ball mills. *Applied Mathematical Modelling*, vol. 16, 1992. pp. 598–604.
3. Mishra, B.K. and Rajamani, R.K. Simulation of charge motion in ball mills: Part 1. Experimental verification. *International Journal of Mineral Processing*, vol. 40, 1994. pp. 171–186.
4. Cleary, P.W. Predicting charge motion, power draw, segregation, wear and particle breakage in ball mills using discrete element methods. *Minerals Engineering*, vol. 11 (11), 1998. pp. 1061–1080.
5. Cleary, P.W. Charge behaviour and power consumption in ball mills: sensitivity to mill operating conditions, liner geometry and charge composition. *International Journal of Mineral Processing*, vol. 63, 2001. pp. 79–114.
6. Van Nierop, M.A., Glover, G., Hinde, A.L., and Moys, M.H. A discrete element method investigation of the charge motion and power draw of an experimental two-dimensional mill. *International Journal of Mineral Processing*, vol. 61, 2001. pp. 77–92.
7. Djordjevic, N. Discrete element modeling of the influence of lifters on power draw of tumbling mills. *Minerals Engineering*, vol. 16, 2003. pp. 331–336.
8. Rajamani, R.K., Mishra, B.K., Venugopal, R., and Datta, A. Discrete element analysis of tumbling mills. *Powder Technology*, vol. 109, 2000. pp. 105–112.
9. Cleary, P.W. Recent advances in dem modeling of tumbling mills. *Minerals Engineering*, vol. 14, 2001. pp. 1295–1319.
10. Morrison, R.D., Cleary, P.W., and Valery, W. Comparing power and performance trends from DEM and JK modeling. *SAG 2001*, Department of Mining and Minerals Process Engineering, University of British Columbia, Vancouver, 2001. pp. 284–300.
11. Inoue, T. and Okaya, K. Grinding mechanism of centrifugal mills—a simulation study based on the discrete element method. *International Journal of Mineral Processing*, vol. 44–45, 1996. pp. 425–435.
12. Cleary, P.W. and Hoyer, D. Centrifugal mill charge motion and power draw: comparison of DEM predictions with experiment. *International Journal of Mineral Processing*, vol. 59, 2000. pp. 131–148.
13. Thornton, C., Ciomocos, M.T., and Adams, M.J. Numerical simulations of agglomerate impact breakage. *Powder Technology*, vol. 105. 1999. pp. 74–82.
14. Kafui, K.D. and Thornton, C. Numerical simulations of impact breakage of a spherical crystalline agglomerate. *Powder Technology*, vol. 109, 2000. pp. 113–132.
15. Mishra, B.K. and Thornton, C. Impact breakage of particle agglomerates. *International Journal of Mineral Processing*, vol. 61, 2001. pp. 225–239.
16. Potapov, A.V. and Campbell, C.S. Computer simulation of impact-induced particle breakage. *Powder Technology*, vol. 81, 1994. pp. 207–216.
17. Tomas, J., Schreier, M., Groger, T., and Ehlers, S. Impact crushing of concrete for liberation and recycling. *Powder Technology*, vol. 105, 1999. pp. 39–51.
18. Schubert, W., Khanal, M., and Tomas, J. Impact crushing of particle-particle compounds—experiment and simulation. *International Journal of Mineral Processing*, vol. 75, 2005. pp. 41–52.
19. Whittles, D.N., Kingman, S., Lowndes, I., and Jackson, K. Laboratory and numerical investigation into the characteristics of rock fragmentation. *Minerals Engineering*, vol. 19, 2006. pp. 1418–1429.
20. Djordjevic, N., Shi, F.N., and Morrison, R.D. Applying discrete element modeling to vertical and horizontal shaft impact crushers. *Minerals Engineering*, vol. 16, 2003. pp. 983–991.
21. Bergstrom, B.H. Crushability and grindability. *SME, Min-Proc. Handbook*, vol. II, 1985. pp. 3065–3073.
22. Potyondy, D.O. and Cundall, P.A. A bonded-particle model for rock. *International Journal of Rock Mechanics and Mining Sciences*, vol. 41, 2004. pp. 1329–1364.
23. Itasca Consulting Group, Inc. PFC3D Particle Flow Code in 3 Dimensions, Minneapolis, Minnesota, 1999.
24. Itasca Consulting Group, Inc. FLAC3D Fast Lagrangian Analysis of Continua in 3 Dimensions, Minneapolis, Minnesota, 2002.
25. Donovan, J.G. Fracture toughness based models for the prediction of power consumption, product size and capacity of jaw crushers. PhD Thesis, Virginia Polytechnic Institute, USA, 2003.
26. Refahi, A., Rezai, B., and Aghazadeh, J. Use of rock mechanical properties to predict the Bond crushing index. *Minerals Engineering*, vol. 20, 2007. pp. 662–669.
27. Csoke, B., Hatvani, Z., Pabanastassiou, D., and Solymar, K. Investigation of grindability of diasporic bauxites in dry, aqueous and alkaline media as well as after high pressure crushing. *International Journal of Mineral Processing*, vol. 74, 2004. pp. 123–128.
28. Lajtai, E.Z., Duncan, E.J.S., and Carter, B.J. The effect of strain rate on rock strength. *Rock Mechanics and Rock Engineering*, Technical Note, vol. 24, no. 2, 1991. pp. 99-109. ◆